CDF note 9074

Measurement of the $\psi(2S)$ Production Cross Section

The CDF Collaboration
URL http://www-cdf.fnal.gov
(Dated: November 15, 2007)

We present a measurement of the differential production cross section of the $\psi(2S)$ vector meson using 1.1 fb^{-1} data collected in CDF Run II. We use the decay $\psi(2S) \rightarrow \mu^+\mu^-$ and cover the kinematic range 2.0 GeV/$c \leq p_T(\psi(2S)) <$ 30 GeV/c and $|y| \leq 0.6$. We find the integrated cross section for inclusive $\psi(2S)$ production for transverse momenta from 2 to 30 GeV/c in the rapidity range $|y| \leq 0.6$ to be $3.14 \pm 0.04(stat)^{+0.23}_{-0.22}(syst)$ nb. We separate the fraction of prompt $\psi(2S)$ events from the decay of the long-lived b hadrons using the proper decay length distribution. We find the integrated cross section for prompt $\psi(2S)$ production for transverse momenta from 2 to 30 GeV/c in the rapidity range $|y| \leq 0.6$ to be $2.60 \pm 0.05(stat)^{+0.19}_{-0.18}(syst)$ nb.

I. INTRODUCTION

Charmonium production provides a unique laboratory for testing our understanding of quantum chromodynamics (QCD) at the interface of the perturbative and non-perturbative regimes which describe the physics of heavy-quark creation and bound state formation respectively. The so-called color-singlet model initially used to describe these processes has been superseded by a rigourous framework based on the non-relativistic QCD (NRQCD) which is an effective field theory [1]. The CDF Run I measurement of J/ψ and $\psi(2S)$ production cross sections [2] prompted the development of NRQCD models. In general, the model predictions agree well with the measured cross section data after parameters are adjusted. However not all the predictions of the NRQCD factorization approach have been firmly established. Indeed, the recent CDF Run II polarization measurements [3, 4] demand a substantial improvement in theory models to accommodate the polarization data. This analysis will push the p_T range of the $\psi(2S)$ cross section measurement deeper into the perturbative regime than was possible with the Run I data in order to test how well the theoretical models can follow the p_T dependence.

II. DATA SAMPLE & EVENT SELECTION

For this analysis we use data with an integrated luminosity 1.1 fb^{-1} collected during Run II upto February 2006. The data are collected with a dimuon trigger that requires two oppositely charged muons, each muon p_T greater equal than 1.5 GeV/c and the invariant mass of the muons in the range of 2.7 GeV/c - 4.0 GeV/c.

The $\psi(2S) \rightarrow \mu^+\mu^-$ decays are reconstructed by selecting events with two oppositely charged muon candidates reconstructed in the Central Outer Tracker(COT) and Central Muon detector. A muon candidate is triggered by a match between a track found in the COT and a collection of hits in the muon detectors. We added Silicon Vertex Detector information to the candidate tracks in refit process offline. We selected $\psi(2S)$ candidates in the invariant mass window of 3.5 GeV/c^2 - 3.8 GeV/c^2, in the rapidity range $|y(\mu^+\mu^-)| < 0.6$, and in the p_T range 2.0 GeV/c - 30.0 GeV/c.

III. UNBINNED MAXIMUM LIKELIHOOD FIT

An unbinned maximum likelihood fit in candidate mass and proper decay length ct is used to extract the $\psi(2S)$ events from the background events and at the same time separate the prompt and B-decay $\psi(2S)$ yield.

The mass component separates the signal and the background. The signal function for the mass fit is modeled by a Crystal Ball function and a first order polynomial to describe the mass background. The Crystal-Ball function is an empirical probability density function introduced by the Crystal Ball Collaboration [5] to describe distributions with a low-side tail to a Gaussian shape. It consists of a Gaussian core portion and a power-law low-end tail, below a certain mass value.

$$Crystal\ Ball\ Function = \begin{cases} A \cdot e^{-\frac{(Et-Em)^2}{2\sigma^2}} & \text{if } \frac{Em-Et}{\sigma} > -\alpha \\ A \cdot \left(\frac{n}{\alpha}\right)^n \frac{e^{-\frac{\alpha^2}{2}}}{\left(\frac{Et-Em}{\sigma}+\frac{n}{\alpha}-\alpha\right)^n} & \text{if } \frac{Em-Et}{\sigma} \leq -\alpha \end{cases}$$

Em is the fit parameter for the invariant mass centroid and Et is the invariant mass of each event. A is the normalization constant, and empirical parameters α and n describe the tail function.

The separation of promptly-produced $\psi(2S)$ from $\psi(2S)$ originating in the decays of long-lived particles (mostly B decays) is made by a proper time fit. A double Gaussian probability density function is used to describe the prompt component and the long-lived component is modeled by an exponential convoluted by a Gaussian.

$$E \otimes G = \frac{1}{c\tau} exp\left[\frac{\sigma^2}{2c\tau^2} - \frac{x}{c\tau}\right] \cdot \left[1 - Freq\left(\frac{\sigma}{c\tau} - \frac{x}{\sigma}\right)\right] \quad ,$$

where $c\tau$ is the mean of proper decay length, σ is the error of $c\tau$, x is the proper decay length of each event, and $Freq(y)$ is the normal frequency function, $Freq(y) = \frac{1}{\sqrt{2\pi}} \int_{-\infty}^{y} e^{(-t^2/2)}\, dt$.

The background component in the lifetime fit is modeled by the sum of a prompt term (double Gaussian), a symmetric long-lived $(E \otimes G)$ term, a positive-ct long-lived $(E \otimes G)$ term, and a negative-ct long-lived $(E \otimes G)$ term.

The likelihood, L, is defined as

$$\begin{aligned} L &= f_s P_s^{mass}\left(f_p P_p^{ct} + (1-f_p)\, P_{E\otimes G}^{ct}\right) \\ &\quad +(1-f_s) P_{bgnd}^{mass}\left(f_{symm} P_{symm}^{ct} + f_+ P_+^{ct} + f_- P_-^{ct}\right. \\ &\quad \left. +(1-f_{symm}-f_+-f_-) P_p^{ct}\right) \quad , \end{aligned} \tag{1}$$

where

- f_s is the $\psi(2S)$ signal fraction from the total number of candidates in the fit,
- f_p is the fraction of prompt $\psi(2S)$,
- f_{sym} is the fraction of symmetric long-lived background,
- f_+ is the fraction of positive-ct long-lived background,
- f_- is the fraction of negative-ct long-lived background,
- P is the corresponding probability density function(PDF): P_s^{mass} is the normalized ($CrystalBallFunction$ + Gaussian), P_p^{ct} is the normalized double Gaussian, $P_{E\otimes G}^{ct}$ is the normalized exponential convoluted Gaussian, P_{bgnd}^{mass} is the normalized first order polynomial, P_{symm}^{ct} is the normalized function in which an exponential convoluted Gaussian for $Et > 0$ is reflected to the negative region, $(E\otimes G)((H[Et]-H[-Et])\cdot Et)$, where $H[y]$ is the Heaviside step function. P_+^{ct} is the normalized $H[Et]\cdot E\otimes G$, P_-^{ct} is the normalized $H[-Et]\cdot(E\otimes G)(-Et)$, P_p^{ct} is the normalized Gaussian.

The empirical parameters n and α describe the radiative tail of the invariant mass distribution. These parameters are p_T independent and fixed in the fit, using the Monte Carlo sample. In addition, the Gaussian width of the mass fit is fixed to keep the p_T independent radiative tail fraction unchanged when the tail parameters are fixed. The lifetime component separates the promptly produced $\psi(2S)$ from B-decay $\psi(2S)$ events. Although the lifetime doesn't affect the total yield, it directly affects the prompt fraction. Because the non-prompt $\psi(2S)$ events are b-decay daughters the p_T of the $\psi(2S)$ is not simply related to the p_T of the parent B-hadron. These events don't have a predictable lifetime. We allow the fit to define an effective b-decay length which is the same in all p_T bins.

We have divided the p_T-range(2 GeV/c- 30 GeV/c) of $\psi(2S)$ into 25 bins as listed in Table I. In each p_T bin, the signal yield and the prompt fraction have been extracted by the unbinned maximum likelihood fit.

TABLE I: Summary of the unbinned maximum likelihood fit.

$P_T(\psi(2S))$	$< P_T >$	Total	Signal	Prompt	Prompt fraction	B decay
2.0-2.5	2.30	35495	2240.5 ± 115.7	1941.2 ± 139.9	0.866 ± 0.018	299.3 ± 55.1
2.5-3.0	2.77	96473	5729.8 ± 184.2	4816.8 ± 215.9	0.841 ± 0.011	913.0 ± 90.4
3.0-3.5	3.25	118868	7931.8 ± 205.4	6746.9 ± 241.4	0.851 ± 0.008	1184.9 ± 97.4
3.5-4.0	3.75	108198	7853.8 ± 196.4	6535.1 ± 229.8	0.832 ± 0.008	1318.7 ± 99.3
4.0-4.5	4.24	91373	8053.2 ± 183.3	6556.8 ± 212.4	0.814 ± 0.008	1496.4 ± 97.2
4.5-5.0	4.74	72106	7440.6 ± 165.2	6052.5 ± 193.8	0.813 ± 0.008	1388.1 ± 90.3
5.0-5.5	5.24	57055	6273.9 ± 148.2	5087.3 ± 174.0	0.811 ± 0.009	1186.6 ± 81.9
5.5-6.0	5.74	44503	5888.4 ± 133.8	4715.7 ± 157.7	0.801 ± 0.009	1172.7 ± 77.2
6.0-6.5	6.24	35099	5316.4 ± 121.0	4160.1 ± 146.7	0.783 ± 0.010	1156.3 ± 78.3
6.5-7.0	6.74	26908	4447.0 ± 107.6	3516.6 ± 129.1	0.791 ± 0.010	930.4 ± 66.5
7.0-7.5	7.24	20253	3571.5 ± 94.2	2713.0 ± 111.9	0.760 ± 0.011	858.5 ± 63.0
7.5-8.0	7.74	15954	3129.4 ± 84.9	2398.9 ± 101.6	0.767 ± 0.012	730.5 ± 56.3
8.0-8.5	8.24	12103	2510.5 ± 74.9	1785.8 ± 87.5	0.711 ± 0.014	724.7 ± 55.8
8.5-9.0	8.74	9569	2039.8 ± 66.9	1431.4 ± 77.7	0.702 ± 0.015	608.4 ± 50.7
9.0-9.5	9.24	7532	1618.0 ± 59.5	1124.7 ± 69.7	0.695 ± 0.017	493.3 ± 46.4
9.5-10	9.74	6020	1344.9 ± 53.8	938.2 ± 64.1	0.698 ± 0.020	406.7 ± 42.9
10 - 11	10.46	8676	1910.8 ± 64.9	1275.8 ± 74.3	0.668 ± 0.016	635.0 ± 52.5
11 - 12	11.46	5733	1348.9 ± 53.2	900.8 ± 63.3	0.668 ± 0.021	448.1 ± 45.4
12 - 13	12.47	3916	908.6 ± 44.3	584.4 ± 50.4	0.643 ± 0.024	324.2 ± 37.7
13 - 14	13.48	2818	640.2 ± 37.6	382.8 ± 41.6	0.598 ± 0.030	257.4 ± 34.2
14 - 15	14.48	2001	465.0 ± 32.0	271.6 ± 34.6	0.584 ± 0.034	193.4 ± 29.2
15 - 17.5	16.12	3061	584.6 ± 39.0	330.3 ± 42.0	0.565 ± 0.034	254.3 ± 36.9
17.5 - 20	18.61	1671	291.7 ± 28.7	154.4 ± 30.1	0.529 ± 0.051	137.3 ± 28.4
20 - 25	22.08	1462	229.9 ± 27.5	132.2 ± 29.5	0.575 ± 0.060	97.7 ± 25.4
25 - 30	27.09	575	83.6 ± 17.8	53.1 ± 19.6	0.635 ± 0.099	30.5 ± 14.8

IV. ACCEPTANCE AND EFFICIENCIES

A. Acceptance and Trigger Efficiency

The $\psi(2S)$ acceptance is calculated using Monte Carlo events. Since the acceptance depends on the $\psi(2S)$ polarization in each p_T bin, it is important to determine a strategy to define an appropriate polarization function for the acceptance calculation. We have measured both the J/ψ and $\psi(2S)$ polarization [4] in CDF Run II, shown in Figure 1. Statistically, the $\psi(2S)$ polarization result is too weak to use as a reliable polarization estimator for the acceptance correction. Therefore, we ask what information we can get from theory.

Recent theoretical models [9–11] agree that the prompt $\psi(2S)$ polarization should be very similar to the J/ψ polarization. The mechanisms are the same. The NRQCD band for J/ψ polarization shown in Figure 1 lies lower than that for the $\psi(2S)$ because it is diluted by theoretically-predicted feeddown effects from χ and $\psi(2S)$ states, rather than just the prompt prediction, which are the same.

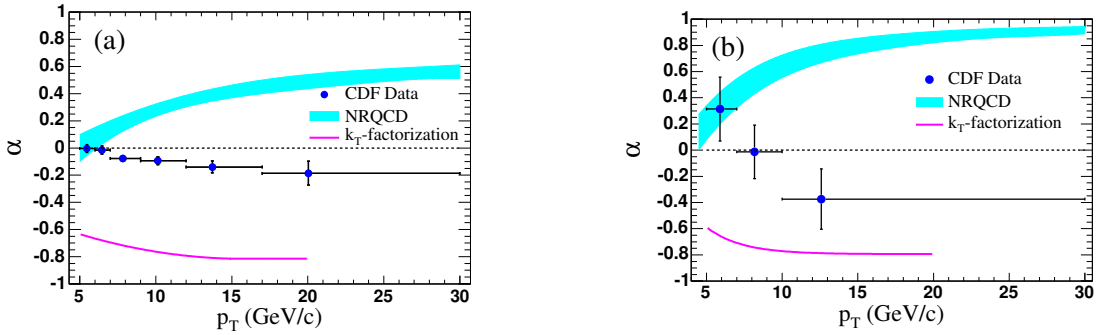

(a) The J/ψ polarization

(b) The $\psi(2S)$ polarization

FIG. 1: The CDF Run II J/ψ and $\psi(2S)$ polarization measurement

We have calculated the χ^2 probability that the $\psi(2S)$ polarization in Fig. 1b is consistent with that of the J/ψ in Fig. 1a. Because the data are binned differently in p_T we fit the J/ψ polarization data to a smooth curve. Using the curve, we compare the mean J/ψ polarization and error at the p_T values of the $\psi(2S)$ measurements. We get the total $\chi^2/ndf = 2.9/3$ (χ^2-probability 0.41) that the two are compatible, as theory would predict. We therefore use the fitted J/ψ polarization central value and error in each of the 25 $p_T(\psi(2S))$ bin to determine the acceptance and its uncertainty.

To calculate the acceptance, we made $\psi(2S)$ MC samples with fixed polarization (0 or -1) and flat distributions in p_T, η and ϕ. After the CDF detector simulation, the events are reconstructed. Detector efficiencies are applied based on data [7]. The combined geometrical acceptance and trigger efficiency, $\mathcal{A}$, is measured by calculating the ratio

$$\mathcal{A} = \frac{N^{rec}(p_T) \times (N^{eff}(p_T)/N^{rec}(p_T))}{N^{gen}(p_T)} \ , \tag{2}$$

where $N^{rec}(p_T)$ is the number of the Monte Carlo events that survived detector geometric and reconstruction requirements, $N^{eff}(p_T)$ is the number of reconstructed Monte Carlo events that pass the randomly-applied trigger inefficiency selection, and $N^{gen}(p_T)$ is the number of the generated events.

The acceptances for each p_T bin with the two extreme $\psi(2S)$ polarization choices are summarized in Table II and shown in Fig. 2. We interpolate to calculate the $\psi(2S)$ acceptance and uncertainty in each p_T bin, using the values from the polarization fit. The effective polarization parameter α_{eff} and the acceptance in each p_T bin are included in the table.

B. Reconstruction Efficiencies

The total reconstruction efficiency is the product of several factors:

$$\epsilon_{reco} = \epsilon^2_{COT} \cdot \epsilon_{SVX} \cdot \epsilon^2_{CMU} \cdot \epsilon^2_{\chi^2} \cdot \epsilon_{z_0} \cdot \epsilon_{\Delta z_0} \quad ,$$

where ϵ_{COT} is the COT-tracking efficiency, ϵ_{SVX} is the SVX II quality cut efficiency, ϵ_{CMU} is the muon reconstruction efficiency in muon chamber, ϵ_{χ^2} is the muon chamber χ^2 cut efficiency, ϵ_{z_0} and $\epsilon_{\Delta z_0}$ are the vertex quality cut

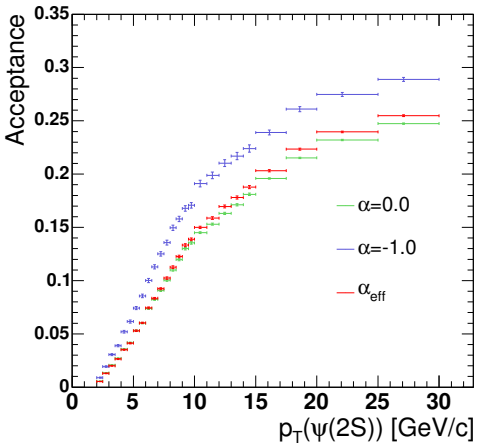

FIG. 2: The acceptance for $\alpha = 0.0, -1.0$ and α_{eff}.

TABLE II: Summary of the effective polarization parameter α_{eff} and the acceptance at α_{eff}.

$P_T(\psi(2S))$	$< P_T >$	α_{eff}	$\mathcal{A}_{eff}$
2.0-2.5	2.30	$0.092^{+0.023}_{-0.054}$	0.0053 ± 0.0002
2.5-3.0	2.77	$0.077^{+0.023}_{-0.050}$	0.0129 ± 0.0003
3.0-3.5	3.25	$0.062^{+0.023}_{-0.046}$	0.0200 ± 0.0004
3.5-4.0	3.75	$0.047^{+0.023}_{-0.042}$	0.0264 ± 0.0005
4.0-4.5	4.24	$0.033^{+0.023}_{-0.039}$	0.0351 ± 0.0006
4.5-5.0	4.74	$0.019^{+0.024}_{-0.036}$	0.0413 ± 0.0006
5.0-5.5	5.24	$0.005^{+0.024}_{-0.033}$	0.0529 ± 0.0007
5.5-6.0	5.74	$-0.008^{+0.025}_{-0.031}$	0.0603 ± 0.0007
6.0-6.5	6.24	$-0.021^{+0.025}_{-0.029}$	0.0744 ± 0.0008
6.5-7.0	6.74	$-0.033^{+0.026}_{-0.027}$	0.0834 ± 0.0009
7.0-7.5	7.24	$-0.045^{+0.027}_{-0.025}$	0.0924 ± 0.0010
7.5-8.0	7.74	$-0.056^{+0.028}_{-0.024}$	0.1024 ± 0.0011
8.0-8.5	8.24	$-0.066^{+0.029}_{-0.023}$	0.1126 ± 0.0012
8.5-9.0	8.74	$-0.077^{+0.030}_{-0.023}$	0.1227 ± 0.0012
9.0-9.5	9.24	$-0.086^{+0.031}_{-0.023}$	0.1333 ± 0.0013
9.5-10	9.74	$-0.096^{+0.033}_{-0.023}$	0.1388 ± 0.0013
10 - 11	10.46	$-0.108^{+0.035}_{-0.024}$	0.1500 ± 0.0011
11 - 12	11.46	$-0.124^{+0.038}_{-0.026}$	0.1587 ± 0.0012
12 - 13	12.47	$-0.137^{+0.042}_{-0.030}$	0.1696 ± 0.0013
13 - 14	13.48	$-0.149^{+0.046}_{-0.035}$	0.1780 ± 0.0014
14 - 15	14.48	$-0.159^{+0.050}_{-0.041}$	0.1878 ± 0.0015
15 - 17.5	16.12	$-0.170^{+0.058}_{-0.054}$	0.2032 ± 0.0010
17.5 - 20	18.61	$-0.178^{+0.073}_{-0.081}$	0.2234 ± 0.0010
20 - 25	22.08	$-0.178^{+0.073}_{-0.081}$	0.2396 ± 0.0008
25 - 30	27.09	$-0.178^{+0.073}_{-0.081}$	0.2548 ± 0.0008

efficiencies. Table III summarizes the offline reconstruction efficiencies which are p_T-independent. The data included in this analysis were collected prior to the significant luminosity increases in February - June, 2006. There are small luminosity-weighted changes included in the efficiencies quoted, as described in the notes.

V. LUMINOSITY

This analysis uses a 1.1fb^{-1}data set collected using the dimuon trigger. As the instantaneous luminosity has increased, the unprescaled trigger path was changed to the dynamically prescaled trigger path to cope with the

TABLE III: Summary of reconstruction efficiencies

Selection	Efficiency
COT offline	$\epsilon(p_T > 1.5) = 99.61 \pm 0.02 \pm 0.91\%$
SVX II offline	$95.3 \pm 1.0\%$
Muon offline	$\epsilon(p_T > 2.0) = 96.1 \pm 1.4\%$
${\chi^2}_\mu \leq 9.0$	$99.6 \pm 1.5\%$
$Z_0 \leq 60cm$	$95.6 \pm 0.3\%$
$\Delta z_0 \leq 5cm$	$99.9 \pm 0.2\%$

increased trigger rate.

The Dynamic-Prescale(DPS) trigger selects events with a varying prescale in the course of a run. In order to calculate the correct luminosity for the dynamically prescaled trigger path, we developed the DPS Accounting tool to calculate the effective luminosity in each run section. The effective luminosity for this analysis is 950 pb^{-1}.

VI. CROSS SECTION

The $\psi(2S)$ differential cross section is calculated as following:

$$\frac{d\sigma(\psi(2S))}{dp_T} = \frac{N(\psi(2S))}{\mathcal{A} \cdot \epsilon_{reco} \cdot \int \mathcal{L}dt \cdot \Delta p_T} \quad ,$$

where $d\sigma/dp_T$ is the average cross section of $\psi(2S)$ in the p_T bin integrated over $|y(\psi(2S))| \leq 0.6$, $\mathcal{A}$ is the trigger efficiency combined acceptance, ϵ_{reco} is the reconstruction efficiency, $\int \mathcal{L}dt$ is the integrated luminosity, and Δp_T is the size of the p_T bin.

The inclusive and prompt $\psi(2S)$ cross sections are listed in Table IV, and the differential cross section results with statistical uncertainties are shown in Figure 3 and 4 for the inclusive and prompt $\psi(2S)$ correspondingly.

The differential cross section of $\psi(2S)$ from B-decays is shown in Fig. 5.

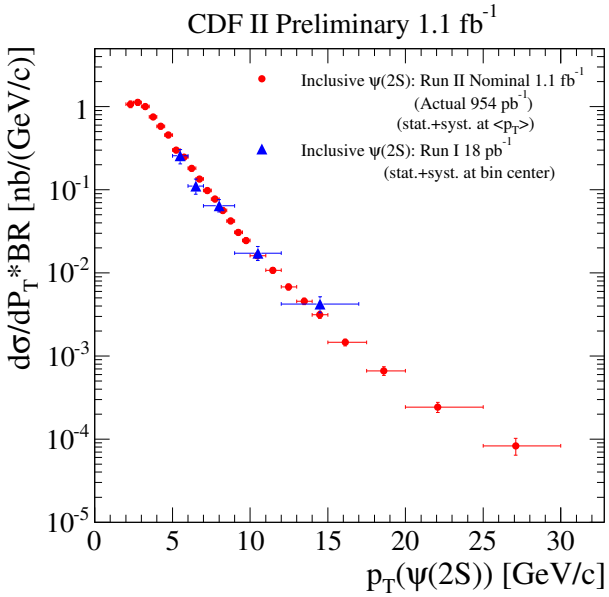

FIG. 3: The inclusive $\psi(2S)$ differential cross section.

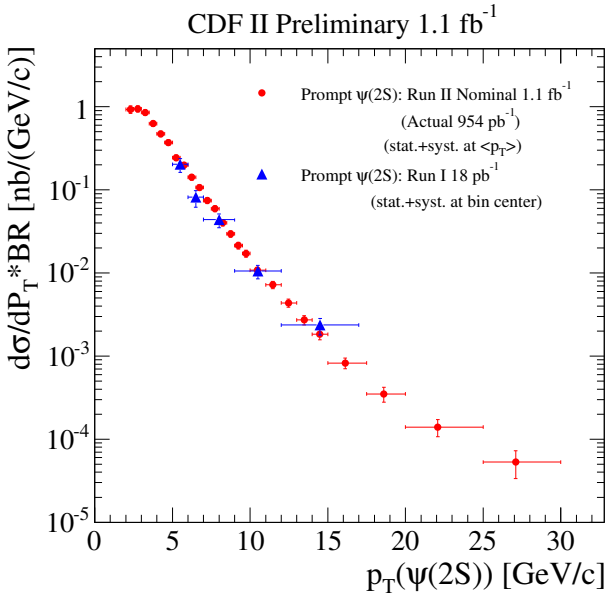

FIG. 4: The prompt $\psi(2S)$ differential cross section.

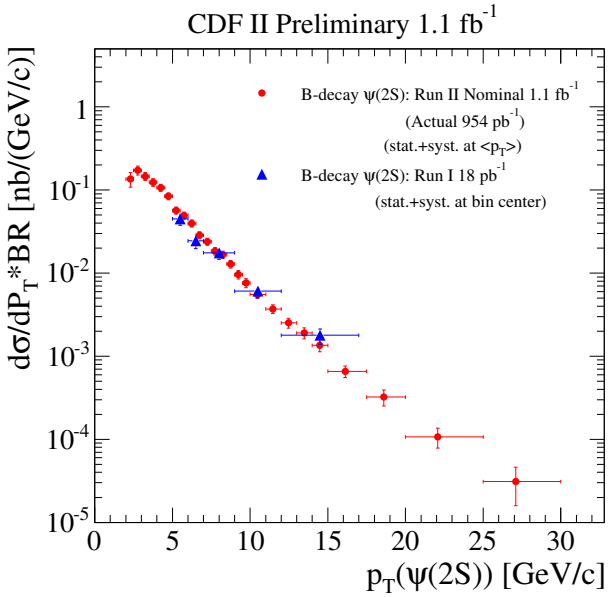

FIG. 5: The $\psi(2S)$ from B-decay differential cross section.

VII. SYSTEMATIC UNCERTAINTIES

The 6% error of the luminosity is the largest systematic uncertainty in this analysis. The systematic uncertainty from the reconstruction efficiency is calculated to be 2.5% from Table III.

In order to estimate the systematic uncertainty from the dimuon trigger efficiencies [7], we vary the trigger efficiency($\epsilon_{trigger}$) by 1σ and look at the changes in the acceptance. The variation depends on p_T.

We have also tried a different mass probability density function (PDF) using a double Gaussian for the mass signal instead of the Crystal Ball function. There was a small yield difference, leading to a mass PDF systematic uncertainty as 0.7%.

Varying the fitting function parameter for B meson decay length produces an error in the prompt fraction of 0.3%.

TABLE IV: The differential cross section times the branching fraction as a function of $p_T$for $|y(\psi(2S))| \leq 0.6$.

$P_T(\psi(2S))$	$< P_T >$	Inclusive $\frac{d\sigma}{dp_T}\cdot$ Br[nb/(GeV/c)]	Prompt $\frac{d\sigma}{dp_T}\cdot$ Br[nb/(GeV/c)]	B-Decay $\frac{d\sigma}{dp_T}\cdot$ Br[nb/(GeV/c)]
2.0-2.5	2.30	$1.071 \pm 0.055\ ^{+0.087}_{-0.080}$	$0.928 \pm 0.067\ ^{+0.076}_{-0.069}$	$0.136 \pm 0.025\ ^{+0.011}_{-0.010}$
2.5-3.0	2.77	$1.125 \pm 0.036\ ^{+0.083}_{-0.079}$	$0.946 \pm 0.042\ ^{+0.070}_{-0.066}$	$0.172 \pm 0.017\ ^{+0.013}_{-0.012}$
3.0-3.5	3.25	$1.005 \pm 0.026\ ^{+0.071}_{-0.068}$	$0.855 \pm 0.031\ ^{+0.060}_{-0.058}$	$0.146 \pm 0.012 \pm 0.010$
3.5-4.0	3.75	$0.754 \pm 0.019\ ^{+0.052}_{-0.050}$	$0.627 \pm 0.022\ ^{+0.043}_{-0.042}$	$0.124 \pm 0.009\ ^{+0.009}_{-0.008}$
4.0-4.5	4.24	$0.581 \pm 0.013\ ^{+0.042}_{-0.041}$	$0.473 \pm 0.015 \pm 0.034$	$0.107 \pm 0.007 \pm 0.008$
4.5-5.0	4.74	$0.456 \pm 0.010 \pm 0.031$	$0.371 \pm 0.012\ ^{+0.026}_{-0.025}$	$0.084 \pm 0.005 \pm 0.006$
5.0-5.5	5.24	$0.301 \pm 0.007\ ^{+0.021}_{-0.020}$	$0.244 \pm 0.008 \pm 0.017$	$0.057 \pm 0.004 \pm 0.004$
5.5-6.0	5.74	$0.247 \pm 0.006 \pm 0.017$	$0.198 \pm 0.007\ ^{+0.014}_{-0.013}$	$0.049 \pm 0.003 \pm 0.003$
6.0-6.5	6.24	$0.181 \pm 0.004 \pm 0.012$	$0.142 \pm 0.005 \pm 0.010$	$0.040 \pm 0.003 \pm 0.003$
6.5-7.0	6.74	$0.135 \pm 0.003 \pm 0.009$	$0.107 \pm 0.004 \pm 0.007$	$0.029 \pm 0.002 \pm 0.002$
7.0-7.5	7.24	$0.0979 \pm 0.0026 \pm 0.0066$	$0.0744 \pm 0.0031 \pm 0.0050$	$0.0239 \pm 0.0018 \pm 0.0016$
7.5-8.0	7.74	$0.0774 \pm 0.0021 \pm 0.0053$	$0.0594 \pm 0.0025 \pm 0.0041$	$0.0184 \pm 0.0014 \pm 0.0013$
8.0-8.5	8.24	$0.0565 \pm 0.0017 \pm 0.0038$	$0.0402 \pm 0.0020 \pm 0.0027$	$0.0167 \pm 0.0013 \pm 0.0011$
8.5-9.0	8.74	$0.0421 \pm 0.0014 \pm 0.0029$	$0.0296 \pm 0.0016 \pm 0.0020$	$0.0129 \pm 0.0011 \pm 0.0009$
9.0-9.5	9.24	$0.0308 \pm 0.0011 \pm 0.0021$	$0.0214 \pm 0.0013 \pm 0.0014$	$0.0096 \pm 0.0009 \pm 0.0007$
9.5-10	9.74	$0.0246 \pm 0.0010 \pm 0.0017$	$0.0171 \pm 0.0012 \pm 0.0012$	$0.0076 \pm 0.0008 \pm 0.0005$
10 - 11	10.46	$0.0161 \pm 0.0005 \pm 0.0011$	$0.0108 \pm 0.0006 \pm 0.0007$	$0.0055 \pm 0.0005 \pm 0.0003$
11 - 12	11.46	$0.0108 \pm 0.0004 \pm 0.0007$	$0.00719 \pm 0.00051 \pm 0.00049$	$0.00371 \pm 0.00038 \pm 0.00025$
12 - 13	12.47	$0.00679 \pm 0.00033 \pm 0.00046$	$0.00437 \pm 0.00038 \pm 0.00030$	$0.00252 \pm 0.00029 \pm 0.00017$
13 - 14	13.48	$0.00456 \pm 0.00027 \pm 0.00031$	$0.00273 \pm 0.00030 \pm 0.00019$	$0.00191 \pm 0.00025 \pm 0.00013$
14 - 15	14.48	$0.00314 \pm 0.00022 \pm 0.00021$	$0.00183 \pm 0.00023 \pm 0.00012$	$0.00135 \pm 0.00020 \pm 0.00009$
15 - 17.5	16.12	$0.00146 \pm 0.00010 \pm 0.00010$	$0.000824 \pm 0.000105 \pm 0.000056$	$0.000658 \pm 0.000095 \pm 0.000045$
17.5 - 20	18.61	$0.000662 \pm 0.000065\ ^{+0.000046}_{-0.000045}$	$0.000350 \pm 0.000068 \pm 0.000024$	$0.000323 \pm 0.000067 \pm 0.000022$
20 - 25	22.08	$0.000243 \pm 0.000029 \pm 0.000017$	$0.000140 \pm 0.000031 \pm 0.000010$	$0.000107 \pm 0.000028 \pm 0.000007$
25 - 30	27.09	$0.000083 \pm 0.000018 \pm 0.000006$	$0.000053 \pm 0.000019 \pm 0.000004$	$0.000031 \pm 0.000015 \pm 0.000002$

As discussed in Section IV, the systematic uncertainty due to the $\psi(2S)$ polarization is estimated from the J/ψ polarization. We interpolate the acceptances from MC samples with $\alpha = -1$ and $\alpha = 0$ using the fitted J/ψ polarization error curves to produce α_{eff}. The change in acceptance due to $\sigma_{\alpha_{eff}}$ is the systematic error.

The fit parameters for mass signal model and B meson decay length have been varied simultaneously and the changes in signal yield have been considered as a systematic error.

All the systematic uncertainties are summarized in Table V.

TABLE V: Summary of the systematic uncertainty.

Source	Systematic Uncertainty
Luminosity	$\pm 6\%$
Reconstruction Efficiency	$\pm 2.5\%$
Trigger Efficiency	$\pm(1.2 - 3.1)\%$
Mass PDF	$\pm 0.7\%$
Prompt Fraction	$\pm 0.3\%$
$\psi(2S)$ Polarization	$\pm(0.7 - 3.8)\%$
Mass and Lifetime Modeling	$\pm(0.2 - 0.5)\%$

VIII. CONCLUSION

We have measured the differential $\psi(2S)$ cross section with 1.1 fb^{-1} CDF Run II data. The measured differential cross section for inclusive and prompt $\psi(2S)$ is summarized in Table IV and shown in Figure 3 and Figure 4.

The integrated cross section is measured to be:

$$\sigma(p\overline{p} \to \psi(2S)X, |y(\psi(2S))| < 0.6,\ p_T > 2\ \text{GeV}/c)_{\sqrt{s}=1.96\ \text{TeV}} \cdot Br(\psi(2S) \to \mu^+\mu^-) = 3.141 \pm 0.038(\text{stat})^{+0.225}_{-0.218}(\text{syst})\ \text{nb}.$$

In the CDF Run I, the inclusive $\psi(2S)$ cross section is measured for $p_T(\psi(2S))$ exceeding 5 GeV/c:

$$\sigma(p\overline{p} \to \psi(2S)X, |\eta| < 0.6, p_T > 5 \text{ GeV}/c)_{\sqrt{s}=1.80 \text{ TeV}} \cdot Br(\psi(2S) \to \mu^+\mu^-) = 0.571 \pm 0.036(\text{stat})^{+0.082}_{-0.089}(\text{syst}) \text{ nb}$$

To compare with the Run I measurement, we have integrated cross section of inclusive $\psi(2S)$ with $p_T > 5$ GeV/c. The cross section is found to be:

$$\sigma(p\overline{p} \to \psi(2S)X, |y(\psi(2S))| < 0.6, p_T > 5 \text{ GeV}/c)_{\sqrt{s}=1.96 \text{ TeV}} \cdot Br(\psi(2S) \to \mu^+\mu^-) = 0.645 \pm 0.006(\text{stat}) \pm 0.044(\text{syst}) \text{ nb}$$

These measurements show that the integrated cross section has increased by 13% compared to the Run I measurement. This is quite consistent with the prediction in the reference [13] of an increase of 1.14 ± 0.08 for prompt J/ψ and $\psi(2S)$ integrated cross sections when the Tevatron center of mass energy is raised from 1.80 to 1.96 TeV.

Acknowledgments

We thank the Fermilab staff and the technical staffs of the participating institutions for their vital contributions. This work was supported by the U.S. Department of Energy and National Science Foundation; the Italian Istituto Nazionale di Fisica Nucleare; the Ministry of Education, Culture, Sports, Science and Technology of Japan; the Natural Sciences and Engineering Research Council of Canada; the National Science Council of the Republic of China; the Swiss National Science Foundation; the A.P. Sloan Foundation; the Bundesministerium für Bildung und Forschung, Germany; the Korean Science and Engineering Foundation and the Korean Research Foundation; the Science and Technology Facilities Council and the Royal Society, UK; the Institut National de Physique Nucleaire et Physique des Particules/CNRS; the Russian Foundation for Basic Research; the Comisión Interministerial de Ciencia y Tecnología, Spain; the European Community's Human Potential Programme; the Slovak R&D Agency; and the Academy of Finland.

[1] G. T. Bodwin, E. Braaten, and G. P. Lepage, Phys. Rev. D **51**, 1125 (1995); Erratum, *ibid.* Phys. Rev. D **55**, 5853 (1997); E. Braaten and S. Fleming, Phys. Rev. Lett. **74**, 3327 (1995).
[2] CDF Collaboration, J/ψ and $\psi(2S)$ Production in $p\overline{p}$ collisions at $\sqrt{s} = 1.8$ TeV, Phys. Rev. Lett. **79**, 572 (1997).
[3] CDF Collaboration, T. Affolder *et al.*, Measurement of J/ψ and $\psi(2S)$ Polarization in $p\overline{p}$ collisions at $\sqrt{s} = 1.8$ TeV, Phys. Rev. Lett. **85**, 2886 (2000).
[4] CDF Collaboration, Polarization of J/ψ and $\psi(2S)$ Mesons Produced in $p\bar{p}$ Collisions at $\sqrt{s} = 1.96$ TeV, Phys. Rev. Lett. **99**, 132001 (2007).
[5] Gaiser, J., CHARMONIUM SPECTROSCOPY FROM RADIATIVE DECAYS OF THE J/ψ AND $\psi(2S)$, SLAC-0255 (1982).
[6] W.-M. Yao *et al.*, The Review of Particle Physics, Journal of Physics G **33**, 1 (2006)
[7] D. Glenzinski *et al.*, Measurement of Level 1, 2 and 3 low p_T dimuon efficiencies for the $B_s \to \mu^+\mu^-$ analysis, CDF Note 7314 (2007).
[8] Giovanni Punzi, Comments on Likelihood fits with variable resolution, PHYSTAT2003, SLAC Sep. 8-11, 2003.
[9] Sean Fleming and I.Z. Rothstein, Adam K. Leibovich, Power counting and effective field theory for charmonium , Phys. Rev. D **64**, 036002 (2001).
[10] V. A. Khoze, A. D. Martin, M. G. Ryskin, and W. J. Stirling, Inelastic J/ψ and Υ hadroproduction, Eur. Phys. J. C **39**, 163 (2005).
[11] S. P. Baranov, Highlights from the k_T-factorization approach on the quarkonium production puzzles, Phys. Rev. D **66**, 114003 (2002).
[12] CDF Collaboration, Measurement of the J/ψ Meson and b-Hadron Production Cross Sections in $p\bar{p}$ Collisions at $\sqrt{s} =$ 1960 GeV, Phys. Rev. D **71**, 032001 (2005).
[13] Anikeev, K. and others, B physics at the Tevatron: Run II and beyond, e-Print: hep-ph/0201071 (2001).